
Article:
Chandrasekhar, K., Rongong, J. orcid.org/0000-0002-6252-6230 and Cross, E. orcid.org/0000-0001-5204-1910 (2019) Mechanical behaviour of tangled metal wire devices. Mechanical Systems and Signal Processing, 118. pp. 13-29. ISSN 0888-3270

https://doi.org/10.1016/j.ymssp.2018.08.021

Mechanical Behaviour of Tangled Metal Wire Devices

Kartik Chandrasekhar*, Jem Rongong, Elizabeth Cross

Sir Frederick Mappin Building, Mappin Street, Sheffield, S1 3JD, UK.

Abstract

Tangled metal wire (TMW) devices can be used as damping elements in extreme environments where traditional materials such as viscoelastic polymers deteriorate or become ineffective. Dynamic properties of TMW devices are highly nonlinear because the microstructure consists of coiled metal wires that are compressed together. This paper examines the sensitivity of their dynamic stiffness and damping to loading conditions, in particular, pre-compression, dynamic amplitude and frequency of excitation. Using displacement-controlled experiments, it is shown that properties depend strongly on pre-compression and dynamic amplitude as would be expected in a structure comprising many frictional contact points. Frequency dependence is shown to be negligible over a broad frequency range that encompasses the region of interest for typical machine applications. This work identifies slow dynamic effects, with timescales of the order of around 10 seconds, which show that quasi-static testing, which is sometimes used for these materials, will not provide accurate estimates of dynamic properties.

Keywords: damping, hysteresis, friction, quasi-static and dynamic behaviour

1. Introduction

Tangled metal wire (TMW) devices are made by weaving together helically coiled wires and compressing them in a mould to produce a desired shape [1,

*Corresponding author
Email address: k.chandrasekhar@sheffield.ac.uk (Kartik Chandrasekhar)

2, 3]. There is growing interest in employing them as passive vibration control elements because their performance does not degrade in extreme environments. This has led them to be used in spacecraft [4, 5], turbomachinery [6, 7] and cryogenic [8] applications. TMW devices have been produced using several materials including steel [8], titanium [9], and nickel based superalloys [10]. Remarkably, TMW devices have also been manufactured using shape memory alloys [11].

The vibration behaviour of TMW devices is comparable to equivalent ones made from rubbery polymers and, consequently, they are sometimes referred to as "metal rubber" devices. Their properties are affected by the type of wire used [12] and the microstructure that is created during manufacture. This microstructure is heterogeneous: X-ray scans reveal that it is formed of closely packed, interwoven coils whose distribution and orientation are somewhat inconsistent throughout the volume [13, 14].

As with any dampers used to tackle vibration problems, the mechanical properties of TMW devices rely on their geometrical dimensions. Researchers have found that if the size of the device is large compared to its microstructure, it is reasonable to assume homogeneity [14]. Therefore, stiffness can be obtained directly from the nominal elastic modulus, and the loss factor can be assumed to be constant. However, due to the nonlinear strain dependence, unusual geometries that result in non-uniform strain could provide unexpected behaviour.

Quasi-static, uniaxial load-deflection tests, conducted by many different teams of researchers, show that stiffness increases with compression level and that the load-deflection hysteresis loop is not symmetric. As Poisson's ratio is typically low [13], uniaxial compression results in increased density. It is commonly concluded that compression increases the number of wire-to-wire contacts.

As there are currently no reliable models that can predict dynamic performance based on device construction, successful selection and design of an TMW device for a particular application relies on previous experience, and a certain

amount of trial and error. Much of the current research effort in this field is therefore focused on developing understanding of the mechanisms that govern behaviour, and their relationships to the microstructure. Complicating factors that delay consensus are that performance depends on the characteristics of the dynamic load and that there is inherent variability of the microstructure even for nominally identical specimens. Thus, the explanations provided by different research teams for particular behaviour can appear to be in conflict.

One area where uncertainty remains is the explanation of the way in which energy dissipation is affected by loading. In operation, TMW devices are usually subjected to pre-compression to ensure that they avoid tensile loads that can cause them to disintegrate. Most researchers accept that dynamic behaviour depends on the relative importance of three possible contact conditions between adjacent wire segments: open, sliding and sticking [15]. At very low compression levels, behaviour is dominated by open contacts (i.e. no contact) with deformation occurring in the wires in a linear elastic manner, and therefore energy dissipation is negligible. At very high compression levels, on the other hand, slip at most contacts is eliminated. Loads can exceed plastic limits, causing permanent bending of wires and local deformation at wire-to-wire contacts. Operation is this stage is generally avoided [16]. When the compression level lies in between these extreme conditions, slip can occur at contacts between adjacent coils.

The nature of the sliding contact has been discussed extensively. It is generally accepted that the stiffness reduces somewhat as the dynamic amplitude is increased and that this is caused by slippage at previously sticking contacts. There is less agreement, however, regarding the mechanism by which energy is dissipated. Experimental results showing that the addition of oil to an TMW device reduced the damping negligibly has led some to suggest that the damping may not be Coulombic in nature [17], and should be represented using a hysteretic model [18]. However, a typical hysteresis loop for an TMW device has sharp corners at the extreme displacements indicating that a classical hysteretic model is not appropriate [19]. While models employing combined

Coulomb friction and viscous behaviour have been proposed [19, 20], there is no clear experimental evidence to show that they are any more than convenient phenomenological models that fit specific data sets.

One of the main arguments for including damping of any kind other than Coulomb friction has been to explain frequency dependence evident in some published results. While most published data refers to quasi-static tests, a number of researchers have conducted dynamic tests at different excitation frequencies [16, 19, 21, 10, 22]. Hou *et al.* noted a reduction in damping with increasing frequency over the range 1 to 10 Hz [19]. When studying TMW bearing supports subjected to random vibration loading, Ma *et al.* noted that as frequency increased, the stiffness increased and the damping increased to a maximum before decreasing [21]. Zhang *et al.* tested TMW specimens over a frequency range of 1 to 200 Hz and noted that with increasing frequency stiffness increased significantly while damping reduced only slightly [10]. Zhang, K. *et al.*, however, from evaluating TMW isolators at frequencies up to 3 Hz, stated that frequency did not affect damping behaviour [22].

The lack of agreement regarding performance is significant, as the differing viewpoints cast doubt on any model that is used to represent TMW. Successful models so far have typically been fitted models (for example, see the work by Zhang, B. *et al.* [20]) for particular specimens and input amplitudes. These are limited in value since the parameters in the fitted models, in general, cannot be extended to other TMW devices. The aims of this paper therefore are to investigate the effects of pre-compression, dynamic amplitude and excitation frequency on a set of test specimens and to relate these findings to conclusions made previously.

It should be noted that an extensive study involving these parameters has previously been performed by Zhang *et al.* [10]. In that work, a dynamic mechanical analysis (DMA) machine was used to take measurements. While the results from that study are valuable, particularly because they used a large number of nominally identical specimens to give statistical information such as the standard deviation in properties, a particular limitation was the type

of loading that the equipment could deliver. Tests were conducted under a form of load control, where the actuator provided nominally sinusoidal forcing and the peak amplitude was adjusted to meet set levels. The key difference in the work described here is that closed loop waveform control is applied to the displacement signal. The advantage of this approach is that it allows like-for-like comparisons to be made as the frequency and amplitude of the loading is altered.

2. Methodology

TMW devices are typically designed to have a particular relative density. The relative density, $\tilde{\rho}$ is a measure of ratio of the mass of the specimen divided by the volume of the wires within the microstructure relative to the mass of a solid block of same geometry to its volume. As Zhang *et al.* demonstrated, specimen variability for TMW devices are considerable, with mechanical properties varying as much as 10% [10]. Whilst the results by Zhang *et al.* [10] bears significance, the main objective of this paper is to understand the underlying principles that dictate the mechanical behaviour of TMW devices. To achieve this, displacement controlled quasi-static, low frequency dynamics, and high frequency dynamics tests are carried out on the TMW devices in an effort to observe and understand the changes in the mechanical properties of the TMW devices over a range of inputs. The quasi-static response of the TMW devices helped form the dynamics test plan.

The results presented in this paper consist of 4 washer shaped specimens made of Grade 304 stainless steel wires with a nominal wire diameter of 0.15 mm. Wire-drawing was performed on the initially helical spiral wires, of nominal coil diameter of 1 mm. The drawn wires were then woven, and compressed in a mould. Two specimens had a relative density of 0.18, whereas the other two had a relative density of 0.23. The specimens had an average outer diameter of 18.4 mm, an average inner diameter of 7.79 mm, and an average height of 5.96 mm. In general, the practice of manufacturing TMW devices involves producing

several TMW devices, testing them, and observing if they fit the design criteria. If they do not pass the test, they are disposed.

Figure 1 shows one of the specimens considered in this research work.

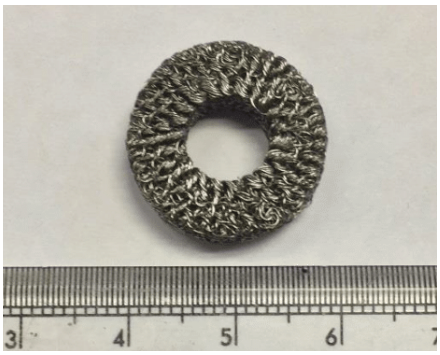

Figure 1: Tangled metal wire device

Hysteresis curves of linear systems have traditionally been associated with a nominal stiffness coefficient and a loss factor. As it has been briefly discussed in the literature survey of Section 1, and will be seen in more detail in this paper, the hysteretic behaviour of TMW devices is nonlinear and the hysteresis curves are asymmetrical. As there are no standard guidelines regarding the analysis of nonlinear hysteretic systems, the behaviour of TMW devices were analysed in terms of an average stiffness coefficient, and an effective loss factor. The procedure to obtain these quantities is listed below.

1. The origin for the force and displacement values was reset half way between the maximum and minimum values.
2. The force-displacement hysteresis curve was "split" into 100 distinct vertical slices across the span of the displacement axis. A mean value was then obtained for each slice.
3. The elastic part of the curve was estimated by fitting a polynomial through the average values for each slice generated in Step 2. This can be seen as the solid black curve in Figure 2. The stiffness at any point is the derivative of the polynomial equation, and the average stiffness coefficient

was defined as the stiffness at the midpoint of the hysteresis curve. The order of the fit was based on the overall shape of the hysteresis curve. In the work presented here, a 5^{th} order polynomial was considered adequate. It was noted that higher order polynomials were more sensitive to variance in the data.

4. The energy dissipated per cycle (area between the loading and unloading curves) and potential energy (shown in Figure 2 as the shaded grey area) were calculated by trapezoidal numerical integration.

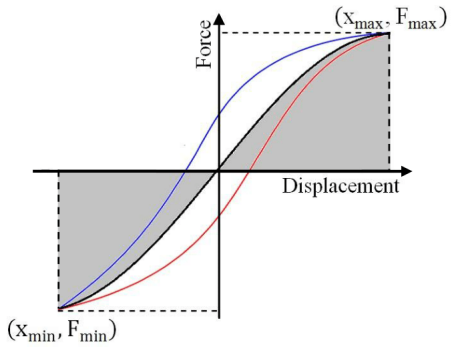

Figure 2: Example of a hysteresis curve with origin beginning at the midpoint of force-displacement data

The loss factor η is a measure of the damping capacity of a material and is commonly defined as,

$$\eta = \frac{\triangle W}{2\pi U} \tag{1}$$

where the numerator, $\triangle W$ is the energy loss per cycle and U is the maximum energy stored during the cycle. However, this cannot be used directly with a TMW specimen that is subject to vibration around a pre-compressed equilibrium condition because the hysteresis loops may be unsymmetrical. Instead, by considering the stored energy either side of equilibrium, with reference to Figure 2, it is possible to write,

$$U = \frac{1}{2}\Big(\int_{x_{min}}^{0} F(x)dx + \int_{0}^{x_{max}} F(x)dx \Big) \tag{2}$$

where $F(x)$ is the function of force, F, with respect to displacement, x. Note that U is now the average peak stored energy. In this work, the values of $\triangle W$ and U were obtained numerically using trapezoidal integration.3

3. Quasi-static behaviour

The term quasi-static used in this paper refers to loading rates on a material where inertial and rate-dependent forces can be ignored. Steady state, quasi-static tests were carried out on washer shaped TMW specimens using a 5 kN hydraulic test machine.

3.1. Experiment

The MTS system applies displacement controlled compressive loading using a hydraulic ram. Data acquisition captured the force and displacement time histories at a rate of 800 samples per second.

Based on recommendations from other researchers, the maximum applied strain on the specimens was restricted to 0.1, although noting that pre-conditioning exercises were performed on all specimens to nominal strains of 0.12. Therefore, compression was applied to a maximum of 0.6 mm, at a rate 0.006 mm/s. The specimens were then unloaded at the same rate. There were small changes to the specimen height after the first quasi-static loading and unloading cycles. These changes were partially attributed to flattening of the uneven TMW surfaces. Previous research, reported by Chandrasekhar *et al.* [23], had shown much more drastic changes in specimen dimensions than those observed in this present research. In the original work, specimens were tested with no prior pre-conditioning, and also with no knowledge of previous loading histories. The pre-conditioning exercises on each of the tested specimens helped to curtail dimension changes. Since the specimens had already undergone compression to

higher loads, applying lower strains to the specimen produced more repeatable results.

The tests were carried out three times to ascertain repeatability of each specimen. For the first load/unload cycle, a pre-compression force of 20 N was applied for each specimen. This ensured that there was complete contact between the surfaces of the hydraulic ram and specimens tested. For the succeeding set of experiments on each specimen, the starting position of the hydraulic ram and the compression displacements were maintained, noting that there was a negligible change in specimen dimensions after the first cycle.

3.2. Results and Discussion

A typical displacement time history from the quasi-static testing carried out is shown in Figure 3 for relative density, $\tilde{\rho} = 0.18$, Specimen 1. It can be seen that after each load increment, the specimen was allowed to dwell for 10 seconds to allow properties to stabilise. Figure 4 illustrates the corresponding force time history for the same specimen. Noise on the raw force signal was noticeable but as the standard deviation was approximately 0.8 N, it was decided that the data collected were acceptable for these investigations. It should be noted that the measured signal which was considered to contain noise may have also contained the response of the specimens undergoing local slip within the microstructure. As the experimental procedures for the rest of the specimens are identical, the respective time histories of displacement and force are not shown.

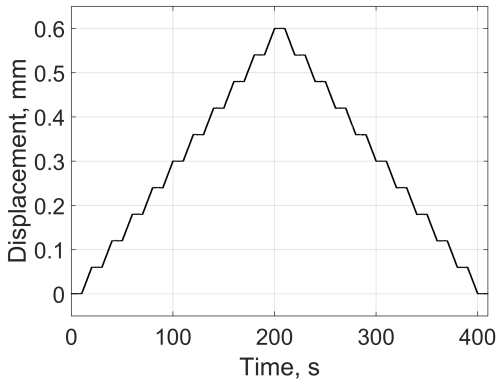

Figure 3: Quasi-static displacement time history for $\tilde{\rho} = 0.18$, Specimen 1

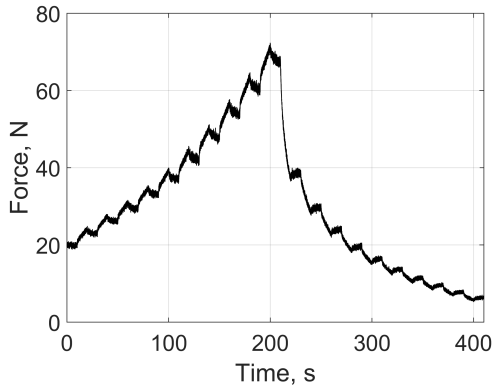

Figure 4: Quasi-static force time history for $\tilde{\rho} = 0.18$, Specimen 1

After each load increment in Figure 4, relaxation occurs in an exponential manner, and as the loads are increased, the magnitude of the relaxation in the force signal increases. This can be explained by the fact that the compressive forces cause the number of contacts in the microstructure to increase, restricting the rate at which the wires reorganise their positions. The relaxation process has a time constant of approximately 6 seconds. This time constant was considered to be the duration for the static force response to become stable, within the bounds of the noise threshold.

There is a significant decrease in force after the first unloading step, and

as the specimen is unloaded further, there is a drop in the rate by which the force reduces. The relaxation phenomenon also occurs when the specimen is unloaded, but this occurs in the opposite direction, with a similar trend as in the loading stage i.e. the magnitude of the relaxation and relaxation time is higher at higher loads. It can be observed that the magnitudes of the relaxation effects in the loading and unloading stages are different. An explanation for this is that the wires, which store energy from the deformations, are 'locked' in position by friction at the contact interfaces. They can only be released if a force greater than the friction force holding them in place is supplied. The restoring forces are not greater than the friction forces, and hence, the specimen 'sets'. That is, the geometric conditions of the specimen after the load has been applied is different than the original geometric condition. It is interesting to note here that the possibility of the contacts being released due to a different loading input was previously noted when a specimen regained its original geometric configuration after being accidentally dropped [23].

Figure 5 illustrates the quasi-static force-displacement hysteresis curves of all the tests conducted on Specimen 1. The curve labelled 'Test 1' corresponds to the data from Figures 3 and 4 plotted against each other.

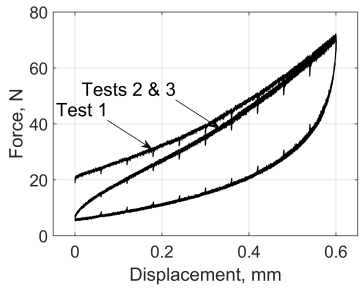

Figure 5: Quasi-static force-displacement curves for $\tilde{\rho} = 0.18$, Specimen 1, Tests 1, 2, and 3

The 20 N pre-compression load applied to the specimen at the start of the loading stage for Test 1 is seen in Figure 5. The force returned to a value of 5 N when the ram returned to its initial position. The starting point of the compressive loading for the second, and third experiments carried out on

the specimens were the same as in the first experiment even though the pre-compressive load had reduced.

It is also seen that the loading starts and unloading stops at a force of 5 N for both Tests 2 and 3, indicating that no further change in the geometric dimensions of the specimen had taken place. It can be seen that there is a change in stiffness between Tests 1 and 2, which is attributed to the pre-compressive load being applied. The results for Tests 2 and 3 indicate similar stiffness characteristics - both in loading and unloading. Pre-compressing the specimen to a higher load in the first load/unload cycle enforced the surface to be even, and when unloaded and reloaded, the results were highly repeatable.

The relaxation effect mentioned previously is seen as spikes on the hysteresis curves. As the specimen is loaded, its stiffness gradually increases nonlinearly. However, the nonlinearity of the loading curve is moderate, when compared to the unloading curve. The largest changes in stiffness occur when the specimen is at its greatest deflection.

An explanation for the observed results is as follows: while the material is being incrementally deformed, new contacts are created within the microstructure, and each wire interface possesses a contact force. Some part of the microstructure deforms elastically, whereas other parts deform in a plastic-like (or quasi-plastic) manner. The quasi-plastic behaviour is seen as a result of the friction locking of the wire interfaces following the application of a load, plasticity occurring at the contact interfaces, as well as plasticity in the individual wires due to bending and torsion. Since the loading is shared in the microstructure, the overall stiffness increase is gradual. The microstructure at maximum displacement has more contacts and contact forces when compared to the undeformed state. When the loads are released, the spring-like nature of the elastic wires cause part of the microstructure to go back to its original state. This causes the number of contacts, and contact forces, to drop rapidly. This in turn causes the stiffness to drop. In parallel to this process, the part of the microstructure that is quasi-plastic also begins to unload. However, as this process is slower, the rate of change of the number of contacts, and contact

forces, decreases as the specimen is unloaded, thereby causing the reduction in stiffness to be gradual.

Figure 6 shows the quasi-static test results for the remaining specimens. It is clear the hysteretic path followed by each specimen is nearly identical.

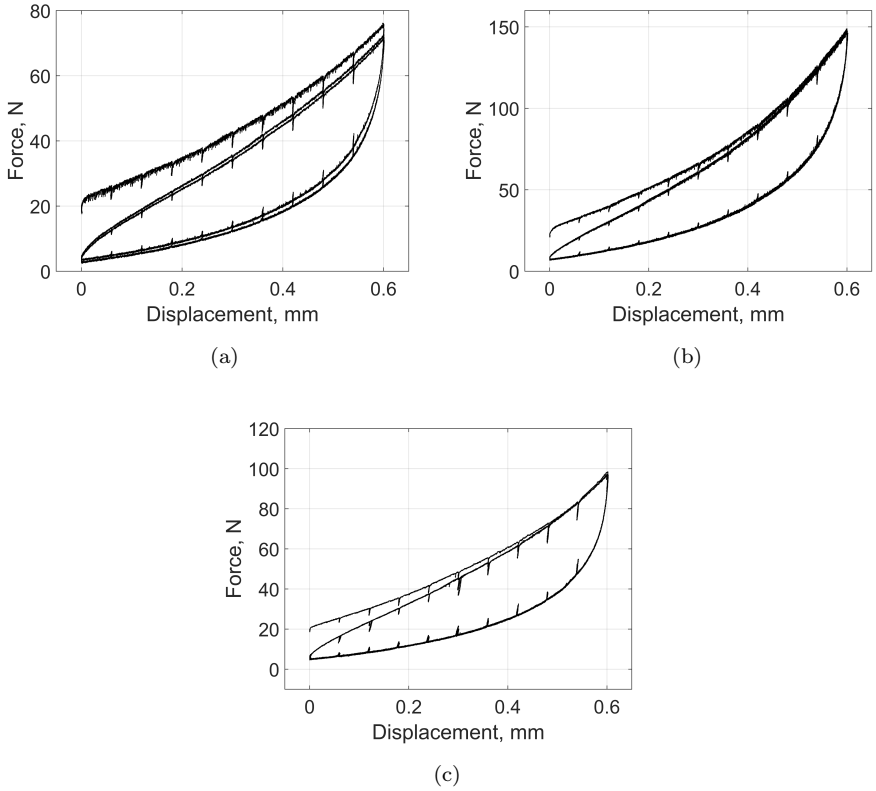

Figure 6: Quasi-static force-displacement curves of all tests performed on: (a) $\tilde{\rho} = 0.18$, Specimen 2, (b) $\tilde{\rho} = 0.23$, Specimen 1, and (c) $\tilde{\rho} = 0.23$, Specimen 2

Table 1 summarises the average coefficients of stiffness calculated for the results shown in Figures 5 and 6. Note that the stiffness coefficients were not computed for the first tests of each TMW specimen since the hysteresis curves were not complete, as seen in Figures 5 and 6.

Relative Density, $\tilde{\rho}$	**Specimen ID**	**Average Stiffness, N/mm**	
		Test 2	**Test 3**
0.18	1	73.9	72.3
	2	77.6	76.7
0.23	1	152.1	154.0
	2	95.2	96.6

Table 1: Estimated average coefficients of stiffness of quasi-static tests performed on the respective specimens

It is noted that the differences in the average coefficients of stiffness for the specimens with the higher relative density ($\tilde{\rho} = 0.23$) are considerable. These differences are attributed to the variability in the microstructural conditions that occur when the TMW devices are woven before they are compressed in the mould. Therefore, it is expected that devices produced under similar conditions may have varying mechanical properties.

4. Dynamic Behaviour

Rate-dependent or inertial effects alter the properties of many damping materials. To understand the significance of these factors, testing was carried out under different loading conditions. This section examines both the low frequency (where frequencies are below 20 Hz), and high frequency (where frequencies range between 50 Hz and 400 Hz) behaviour of TMW devices.

4.1. Hypotheses being tested

Prior to the dynamics experiments, the following hypotheses for the average dynamic stiffness and loss factor were proposed.

4.1.1. Average dynamic stiffness

For the average dynamic stiffness, it was hypothesised that:

1. An increase in the number of contacts, and formation of new contact forces as the pre-compression increases leads to an increase of the average dynamic stiffness coefficient for a given dynamic displacement.
2. When a specimen is maintained at a given pre-compression, wires are forced to travel a greater distance as the dynamic strain is increased. This results in a reduction of the average dynamic stiffness coefficient for the specimen.
3. It has been established that when a specimen is externally loaded, the microstructure densifies. When densification occurs for any given wire under consideration within the microstructure, it requires that other neighbouring wires cooperatively adjust their positions for the wire under consideration to occupy a new space/void within the microstructure. This is a slow relaxation process that is proportional to the density of the microstructure [24]. An increase in the frequency causes the wires to oscillate at faster rates. This reduces the time for the slow relaxation processes to take place. Therefore an increase in specimen stiffness should be observed.

4.1.2. Loss factor

When TMW devices are at equilibrium, the contacts within the microstructure remain in a "stick" state. As loading occurs, a transition between "stick" to "slip" occurs. This transition may not occur across the entire microstructure simultaneously, with some regions slipping more than others. Under the assumption that the primary energy dissipation mechanism in TMW devices is friction, it is hypothesised that:

4. An increase in the static displacement causes the formation of several new contacts between the wires in the microstructure. When the specimen is subjected to oscillatory motion, the contacts begin to move relative to each other, and sliding takes place. This should cause an increase in the loss factor. However, if the specimen is pre-compressed beyond a critical threshold, the large number of contacts within the microstructure may restrict sliding, and so the loss factor will drop. Furthermore, referring

to Equations 1 and 2, as the dissipated energy increases by $O(x)$ and the strain energy increases by $O(x^2)$, the loss factor will eventually reduce after a critical static displacement level is surpassed.

5. As the dynamic displacement increases whilst the static compression is maintained, the contacts are forced to slide over a longer distance. As stated in the previous hypothesis, once a critical dynamic displacement is exceeded, the loss factor may reduce due to the relationship between the dissipated energy and the strain energy.

6. The short term relaxation effects occurring within the microstructure introduce a lag into the response of the microstructure. This lag aids in increasing the loss factor. However, as the frequency is increased, the rapid motion of the microstructure will mitigate the effects of the lag, and thus, the loss factor would reduce.

4.2. Low Frequency Behaviour

The MTS test system discussed in Section 3 was also employed for this work. The system was used to apply prescribed displacements with a sinusoidal waveform at four frequencies: 1 Hz, 3 Hz, 10 Hz, and 20 Hz. The amplitudes of the static and dynamic strains that were applied during these tests are shown in Table 2. Testing was conducted using displacement control as with the quasi-static testing.

Static Strain	**Dynamic Strain**
1%	1%, 2%
5%	1%, 2%, 5%
9%	1%, 2%
1% (unloading)	1%, 2%

Table 2: Range of static strains and dynamic strains examined

4.2.1. Experiment

An example of the displacement time history of the experiments can be seen in Figure 7.

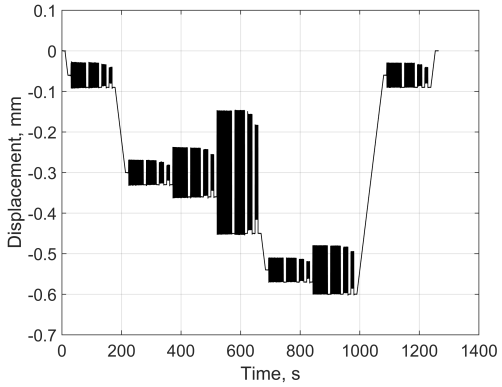

Figure 7: Displacement time history of dynamic test data

The specimens were allowed to relax between each load increment for 10 seconds. The applied strain rate for the ramp load in between experiments was 0.001/s. This allowed a comparison to be made regarding the changes in properties before and after the core dynamic testing.

In order to allow the specimen to stabilise, the test was run for a number of cycles, depending on the frequencies being tested. These can be summarised in Table 3. Approximately, the last 20 cycles for each excitation frequency were considered for the subsequent analysis. This allowed the analysis to be performed on only the steady-state behaviour.

Frequency, Hz	Number of cycles
1	50
3	100
10	150
20	200

Table 3: Number of cycles at the different frequencies tested

At each level of static strain shown in Figure 7, the four frequencies being tested, as well as the various applied dynamic strains, can be seen. It can be seen that as the frequency was increased, the peak value of the dynamic strain reduced for any given applied static strain. This was attributed to the test system exceeding its rated loading capacity. Digital low pass filtering was applied to the displacement and force data to eliminate high frequency noise greater than 10 times the excitation frequency.

The hysteresis curves resulting from the low frequency testing were also nonlinear and asymmetrical, and the results were analysed using the approach described in Section 2.

4.2.2. Results and Discussion

The average dynamic stiffness and loss factors were studied as a function of dynamic amplitude, over the range of static and dynamic loading.

The results for the average stiffness can be observed in Figure 8. Note that, "SS" in the legends stands for static strain. Hence, for example, SS1 stands for 1% static strain.

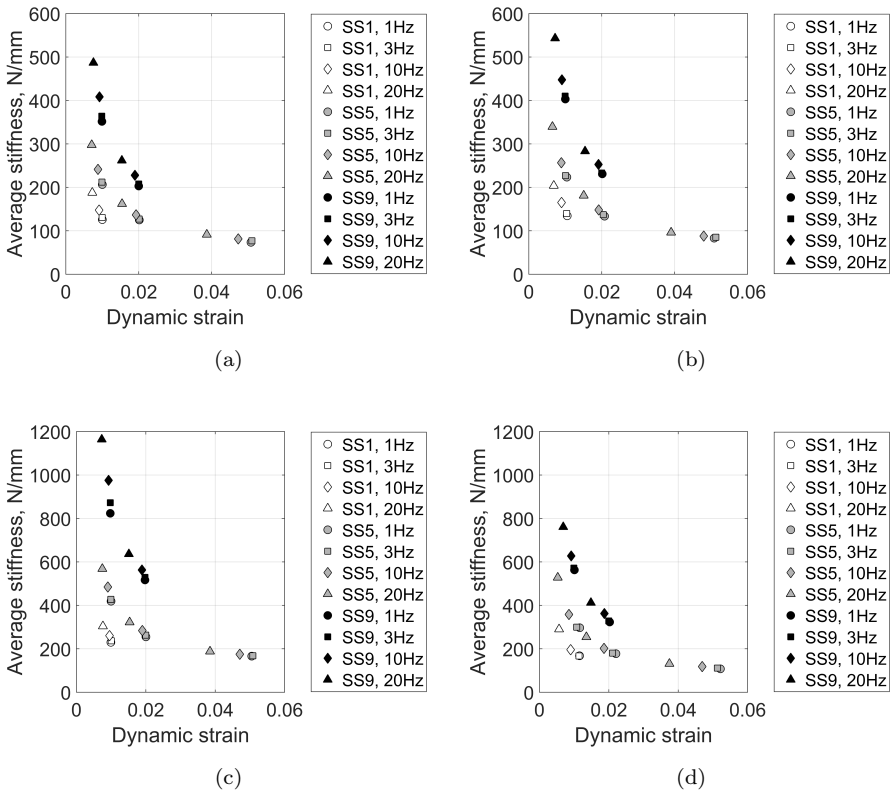

Figure 8: Average stiffness variation with dynamic strain over range of static strains and frequencies for (a) $\tilde{\rho} = 0.18$, Specimen 1, (b) $\tilde{\rho} = 0.18$, Specimen 2, (c)$\tilde{\rho} = 0.23$, Specimen 1, and (d) $\tilde{\rho} = 0.23$, Specimen 2

The results from Figure 8 (a) - (d) show that there are three sets of data that lie on three distinct curves. For a given static strain, results lie approximately along a single curve irrespective of frequency. As the dynamic strain is increased, the average stiffness coefficient is seen to reduce. On the other hand, for a given dynamic strain, the average dynamic stiffness coefficient increases with static strain.

The average stiffness behaviour for all specimens show similar trends. Overall, from the results seen in Figure 8, it can be concluded that the most important parameters affecting the average dynamic stiffness coefficients were the

static (pre-compression) and dynamic strains acting on the specimens. The average stiffness was seen to rise dramatically with a reduction in dynamic strains. Hence, the results are in agreement with Hypotheses 1 and 2. With respect to Hypothesis 3, the effects of frequency were not seen to a significant extent, and it can hence be assumed that there is no obvious frequency dependence, which is a characteristic of Coulomb friction systems. A set of experiments was also performed on the specimens during the unloading process. It was found that the mechanical properties remained consistent (to within 1%).

A comparison of a dynamic hysteresis loop and the equivalent quasi-static one is presented in Figure 9. It can be seen that the dynamic hysteresis loop is slightly thinner, aligning more with the pre-relaxation behaviour seen for the quasi-static hysteresis loop (identified by the inward-pointing spikes in the loop). This indicates that the time periods involved in the dynamic testing (defined by excitation frequency) were above those required for relaxation.

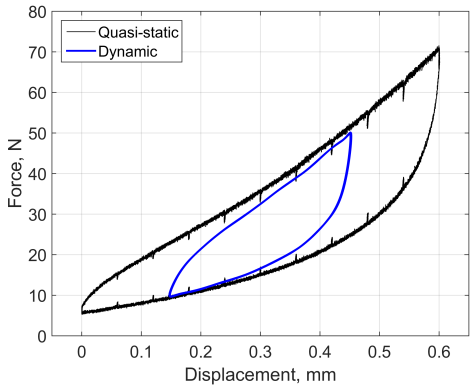

Figure 9: Comparison of quasi-static and dynamic stiffening behaviour at a static strain of 5% and dynamic strain of 5%

Figure 10 (a) - (d) show the loss factor as a function of dynamic strain for all the specimens.

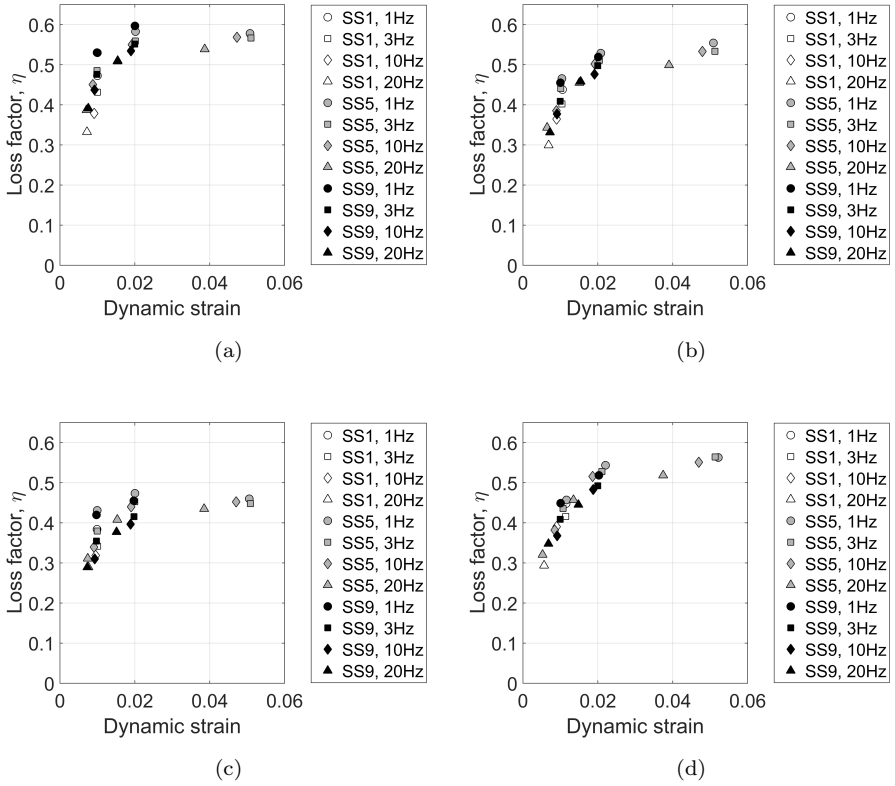

Figure 10: Loss factor variation with dynamic strain over range of static strains and frequencies for (a) $\tilde{\rho} = 0.18$, Specimen 1, (b) $\tilde{\rho} = 0.18$, Specimen 2, (c)$\tilde{\rho} = 0.23$, Specimen 1, and (d) $\tilde{\rho} = 0.23$, Specimen 2

The damping behaviour of all specimens are shown to follow similar trends to each other. It can be seen that the static strain has a small effect on the loss factor. For example, focussing on $\tilde{\rho} = 0.18$, Specimen 1, Figure 10 (a), and considering results at 3 Hz, the loss factor increases from 0.432 to 0.485, and then drops to 0.476 as the static strain is increased from 1% through 5% to 9%. This agrees with Hypothesis 4 and is the expected behaviour for Coulomb friction damping.

The results observed are in agreement with Hypothesis 5. The higher travel of the wires with increased dynamic strain causes an increase in the loss factors.

At high dynamic amplitudes, the loss factor can be seen to reach a plateau. If dynamic amplitudes are increased further, it is expected that loss factors would reduce - in line with expected behaviour for Coulomb friction. This type of behaviour has previously been suggested by Ponomarev [25] (although in that particular work, different loading regimes were considered).

Considering Hypothesis 6, Figure 10 shows that excitation frequency does not appear to have a significant effect on the loss factor over the range considered.

4.3. High Frequency Behaviour

High frequency testing (50 - 400 Hz) was carried out on the same specimens discussed thus far, allowing direct comparisons to be made between the experiments.

4.3.1. Experimental Setup

In order carry out these experimental investigations, a bespoke test structure was designed with the aid of finite element analysis. This structure had to hold the specimen at a set pre-compression and allow dynamic excitation to be applied via an electrodynamic shaker. It was designed so that its lowest natural frequency was above 2.5 kHz. This ensured that the maximum distortion of measured signals caused by structural resonances was less than 1%. The schematic of the test structure, including the vibrating components can be seen in Figure 11. For clarity, the moving (vibrating) components of the test structure are indicated with a textured grey colour.

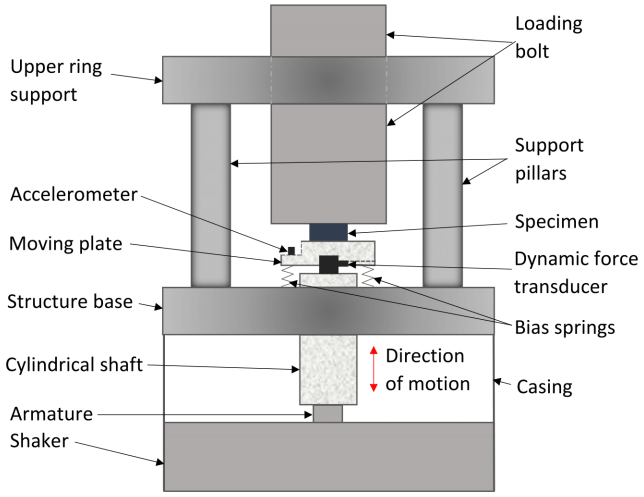

Figure 11: Schematic showing the final setup for the high frequency test structure

The structure comprised four cylindrical support pillars, which connected an upper cylindrical ring support, and the structure base, as shown in Figure 11. The base was attached directly to a DataPhysics V20 electrodynamic shaker. A cylindrical shaft connected the shaker armature to a force transducer, which was then attached to a moving (vibrating) plate. Bias springs, which were placed between the moving plate and the base of the structure, provided restoring forces to specimens. As the plate moved, the deformation of the springs was identical in magnitude but opposite in direction to that experienced by the specimen, which was placed in between the moving plate and the loading bolt. The loading bolt was used to apply pre-compression to the bias springs and the specimen. The moving plate had a recess on one side to accommodate an accelerometer. Some mass was removed on the opposite side of this recess to avoid imbalance on the moving plate as it oscillated.

The results from Section 4.2.2 indicated that the TMW devices were significantly stiff, especially at lower dynamic amplitudes. The choice of the bias spring stiffness coefficient was considered very important in the experimental setup. If a spring with a very low stiffness coefficient were to be chosen, the

specimen would not have been able to be pre-compressed, whereas if the stiffness coefficient was too high, the system response would have been dominated by the springs.

The line diagram in Figure 12 illustrates the flow of data during testing. Data from the accelerometer was fed into a 2^{nd} order low pass Butterworth filter with a cut-off frequency of 1500 Hz. The filter output was then passed to a CompactRIO 9024 input, which was used as a PI controller. Note that the Butterworth filter was only applied to the signal being fed into the control loop, and the filtering procedure on the acquired data was a separate task, which will be discussed in Section 4.3.3.

There were two outputs of the CompactRIO system. The first was the PI controller output, which was sent into the input channel of a Data Physics PA300E 300 W power amplifier. The other output fed the generated ideal sine waveform into the data acquisition system, in the form of a PicoScope 4423 digital oscilloscope. The two other signals which were fed into the PicoScope device were the unfiltered signals from the accelerometer and force transducer, respectively. The ideal sine wave and unfiltered accelerometer signal were used to tune the PI controller. Data acquisition was carried out at a rate of 50 kS/s.

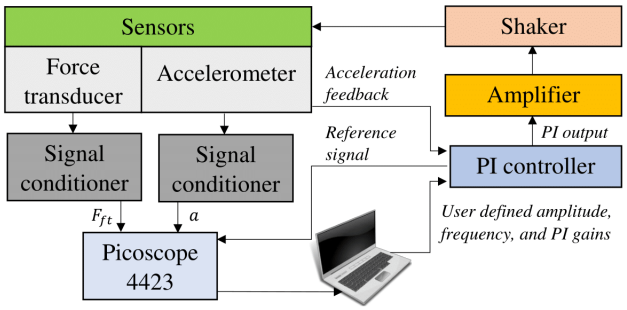

Figure 12: Line diagram of controller and data acquisition system

4.3.2. Experiment

In addition to the study of high frequency behaviour, other characteristics that were investigated included the behaviour at different static compressions, and dynamic amplitudes, similar to those discussed in Section 4.2.1.

The TMW specimens were tested at six frequencies, between 50 Hz and 400 Hz. The range of frequencies (50 - 400 Hz) was a limit imposed due to a combination of:

- the accelerometer used: the acceleration amplitudes for the required displacement amplitudes were very low below 50 Hz.
- the PI controller: the controller performance deteriorated above 400 Hz.

Table 4 summarises the static amplitudes, frequencies, and dynamic amplitudes tested at the corresponding frequencies.

Static Strain	**Frequency, Hz**	**Dynamic Strain**
1% (for higher $\tilde{\rho}$ specimens) 3% (for lower $\tilde{\rho}$ specimens)	50	1%, 2%
	80	1%, 2%
	100	1%, 2%
	200	0.5%, 1%, 2%
	300	0.25%, 0.5%, 1%
	400	0.1%, 0.25%, 0.5%
5% (for all specimens)	50	1%, 2%, 5%
	80	1%, 2%, 5%
	100	1%, 2%, 5%
	200	0.5%, 1%, 2%
	300	0.25%, 0.5%, 1%
	400	0.1%, 0.25%, 0.5%

Table 4: Range of static and dynamic strains examined for the respective frequencies tested

The pre-compression applied to the specimens was estimated from the static deflection of the bias springs. There were some important justifications made from Table 4:

- For the lower relative density specimen, it was noted that with an applied pre-compression strain of 1%, the applied dynamic strains caused a loss of contact between the loading bolt and the specimens being tested. To avoid this, the applied pre-compression was increased to 3% only for the lower relative density specimens.

- At a static strain of 1%, dynamic peak-to-peak amplitudes of up to 2% were tested between 50 Hz and 100 Hz. This ensured that there was no loss of contact between the TMW specimens and the loading bolt holding them in place.

- The dynamic amplitudes were decreased as the frequencies increased because of shaker limitations, although there were overlaps of two dynamic amplitudes for successive frequencies tested.

As with the previous sections, the aim here was to extract the mechanical properties of the TMW devices being tested. However, the presence of the moving plate and the bias springs, illustrated in Figure 11, had an influence the force signals being measured by the force transducer. In order to mitigate these effects, the equation of motion for the moving parts of the test structure had to be manipulated. This equation of motion can be described using Equation 3.

$$m_{mp}a + F_{spr} + F_{spec} = F_{ft} \tag{3}$$

where a is the acceleration signal captured by the accelerometer, m_{mp} is the mass of the moving plate (measured to be 99.93 g using an electronic weighing scale with resolution 0.01 g), F_{spr} and F_{spec} are the restoring forces of the bias springs, and specimen being tested, and F_{ft} is the force trace recorded by the force transducer. In order to remove the inertial forces of the moving plate, and

the restoring forces of the bias springs, and hence extract the properties of the specimen, Equation 3 was rearranged to give,

$$F_{spec} = F_{ft} - m_{mp}a - F_{spr} \tag{4}$$

It was assumed that the entire mass of the moving plate contributed to the dynamic response recorded. It should be noted that in Equations 3 and 4, the inertial term of the specimen mass has been omitted (i.e. $\frac{1}{3}m_{spec}a$). This omission was justified by the fact that the specimen mass was significantly smaller than the mass of the moving plate.

Having discussed the equations of motion for the test structure, it is important to discuss the choice of bias springs. A number of materials were considered for this: natural rubber, wave springs, and helical bias springs. It was found that the natural rubber and wave springs obtained for this work were highly nonlinear, and provided high damping. Whilst the helical springs were also nonlinear, the magnitude of the nonlinearity was significantly smaller, and the damping provided by them was small, and measurable. A total of 8 bias springs were used for all the experiments. Testing was carried out on the helical springs at the frequencies and amplitudes shown in Table 4. The stiffness and damping provided by these bias springs were calculated using the methods shown in Section 2. These were calculated because there may have been internal resonances of the bias springs, in addition to the resonance of the mass-spring system.

Since the bias springs and the specimens were in parallel configuration, the stiffness results for the TMW devices were corrected by subtracting the respective results. The bias spring stiffness coefficients ensured that the TMW specimens being tested were able to be pre-compressed. It was also not too large such that the system response would be dominated by the restoring forces of the springs. Note that although the damping provided by the bias springs was negligible, the calculated loss factors for the TMW devices were also corrected by subtracting the calculated loss factors of the bias spring. Taking the above into consideration, Equation 4 can now be expressed as,

$$F_{spec} = F_{ft} - m_{mp}a - 8k_{spr}x \tag{5}$$

where k_{spr} is the calculated stiffness coefficient of each helical spring, and x is the displacement. In order to obtain the displacement, x, the measured acceleration signal, a was numerically integrated twice with respect to time in postprocessing. The integrated signals were high-pass filtered to remove the constants of integration.

The test structure was validated by testing specimens of natural rubber of known properties. These results are not discussed here in an effort to maintain conciseness. It was found that the Young's modulus of the natural rubber specimen, calculated using the stiffness estimated from the experimental results, was within 10% of the Young's modulus measured directly on a dynamic mechanical analyser machine.

4.3.3. Results and Discussion

With the high frequency test structure validated, the behaviour of the TMW devices were then analysed. The displacement time history for a test performed at 200 Hz is seen in Figure 13, and the corresponding force time history is seen in Figure 14. It should be noted here that the displacements and forces measured were low pass filtered digitally, similar to the data in Section 4.2.1. That is, frequencies 10 times greater than the excitation frequency were removed.

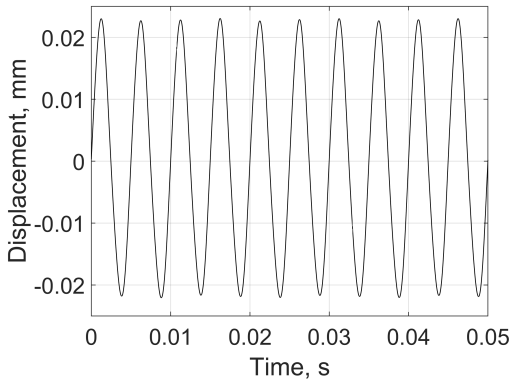

Figure 13: Displacement time history for an experiment carried out at 200 Hz

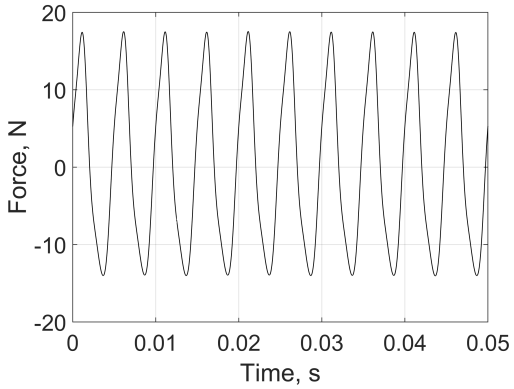

Figure 14: Force time history for an experiment carried out at 200 Hz

The force-displacement hysteresis curve obtained from the data shown above is seen in Figure 15.

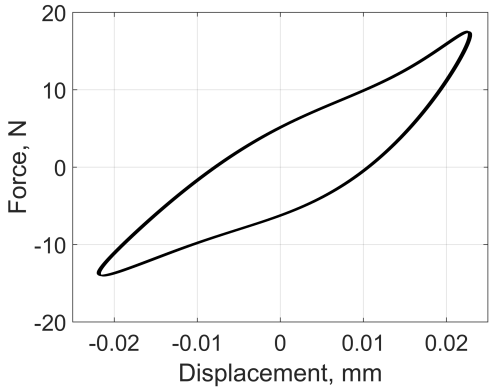

Figure 15: Force-displacement hysteresis curve obtained for the experimental results shown in Figure 13 and 14

The hysteresis curve in Figure 15 appears aesthetically similar, but a lot less asymmetric, to the low frequency hysteresis curves reported in Section 4.2.2. The lower hysteresis curve asymmetry observed in Figure 15 is attributed to the smaller dynamic amplitudes applied to the specimens. This observation helps as an indicator that TMW devices exhibit frequency independence. The results for the average dynamic stiffness and loss factor were once again analysed against the applied dynamic strain. They were scrutinised with respect to the hypotheses proposed in Section 4.1. The frequency dependency, in particular, was an important hypothesis to analyse because it did not particularly have a distinct effect on the reported results in Section 4.2.2. As the frequency was extended to a much larger range in this section, the results reported here have a much higher weighting because inertial effects were more significant at the higher frequencies.

Figure 16 (a) - (d) show the high frequency average stiffness results obtained for a range of dynamic amplitudes and frequencies. The high frequency behaviour is consistent with the behaviour that was previously observed in the quasi-static and low frequency dynamic testing. It is interesting to note that both the lower relative density TMW devices ($\tilde{\rho} = 0.18$) in Figure 16 (a) and (b) behaved very similarly, in that the increase in pre-compression from 3% to

5% did not affect the average stiffness significantly. This was attributed to the fact that the relative increase in pre-compression for the two sets of tests was smaller for the lower relative density specimens than the higher relative density specimens.

Within the range of experimental uncertainty, the frequency dependency hypothesis was, once again, not illustrated in the results, especially when considering the scale of amplitude dependence seen in the results. It is possible that the frequency dependency was not observed in the range considered since the excitation frequencies were much higher than the characteristic frequency of the relaxation processes seen in the quasi-static testing results. In general, average stiffness was shown only to depend on the static pre-compression and dynamic amplitudes of vibration, a characteristic of classical Coulomb friction.

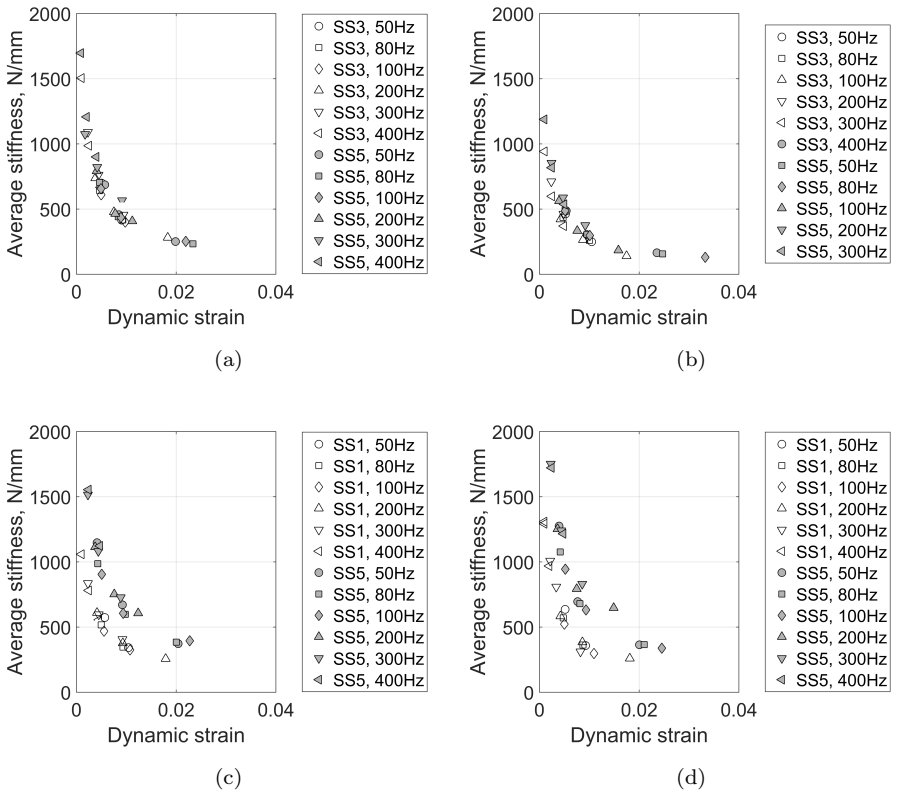

Figure 16: Average stiffness variation with dynamic strain over range of static strains and frequencies for: (a) $\tilde{\rho} = 0.18$, Specimen 1, (b) $\tilde{\rho} = 0.18$, Specimen 2, (c) $\tilde{\rho} = 0.23$, Specimen 1, and (d) $\tilde{\rho} = 0.23$, Specimen 2

Figure 17 (a) - (d) show the high frequency loss factor results obtained for a range of dynamic amplitudes and frequencies.

It was seen that the most important effect on loss factor was that of the dynamic amplitudes of vibration. As the dynamic amplitude increased, the level of damping also increased, but at a decreasing rate. Sufficiently high strains were not achieved to observe the plateaus seen during low frequency testing. The increase of static pre-compression levels, in general, caused higher levels of damping. The frequency dependency hypothesis was not shown for these loss factor results, and therefore, it can be stated that the specimens

tested are independent of frequency in the range considered.

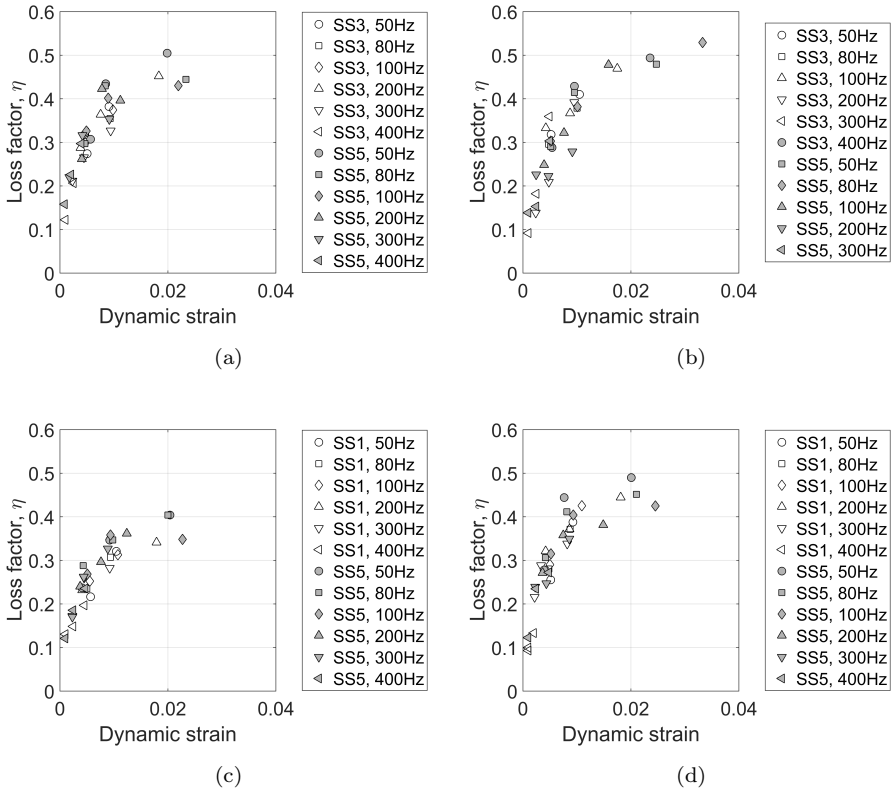

Figure 17: Loss factor variation with dynamic strain over range of static strains and frequencies for: (a) $\tilde{\rho} = 0.18$, Specimen 1, (b) $\tilde{\rho} = 0.18$, Specimen 2, (c) $\tilde{\rho} = 0.23$, Specimen 1, and (d) $\tilde{\rho} = 0.23$, Specimen 2

When compared to the low frequency ($\leq$ 20 Hz) tests, the differences in mechanical properties that can be seen (i.e. average coefficients of stiffness and loss factors) can be explained by the lower dynamic amplitudes that the specimens were subjected to in the high frequency ($\geq$ 50 Hz) tests.

5. Conclusions

TMW devices are inherently nonlinear. Nonlinearity arises both due to friction between contact points within the microstructure, as well as the nonlinear

changes in the number of contacts, and contact areas, formed during load cycles. Nonlinearity due to plasticity may also be a contributing factor. However, this was considered not to be significant because the nominal strain levels were restricted to a maximum of 10%.

The main result from the quasi-static tests revealed that the TMW device microstructure evolves with different loading regimes. The changes in microstructure were somewhat curtailed by the pre-conditioning exercises undertaken, and repeatable force-displacement hysteresis curves were measured. Some relaxation was evident in the specimens as they were subjected to changes in compression levels. On the force-displacement curve, this effect could be seen as spikes facing inward. Because these relaxation effects are essentially short-term, this meant that at higher frequencies, the hysteresis curves became narrower.

For the dynamic testing, the mechanical properties were studied as a function of the dynamic strain. The results were studied according to a number of hypotheses. The trends observed in the high frequency results matched those seen in the low frequency results. Increasing the pre-compression increased the stiffness of the material, in a nonlinear manner. Increasing dynamic amplitudes reduced the stiffness, due to larger travel of the wires in the microstructure. This was also seen to be nonlinear. Increasing the pre-compression increased the loss factor because there are more contacts with higher contact pressures that can slip in the microstructure. Increasing the dynamic amplitude of the cyclic compression also increased the loss factor due to the larger level of slip.

In general, the static and dynamic amplitudes were reported to be the fundamental phenomena driving the performance of the TMW devices. The TMW devices did not show frequency dependence over the range 1 - 400 Hz. The results in this paper show that TMW devices follow classical Coulomb friction behaviour since they are only amplitude dependent over the frequency range studied. This has significant connotations, since modelling of TMW devices can be simplified without having complex frequency dependent terms that researchers have previously included in their models describing TMW devices.

Note that relaxation was evident over a longer timescale than the lowest

frequency of testing (1 Hz). That is, although the timescales of the relaxation effects were short term (less than 10 seconds), they were considered long term when compared to the frequencies being tested. This relaxation is thought to be the result of reorganisation in the microstructure but happens over timescales longer than those associated with vibrations in machinery and components.

Whilst the mechanical properties of TMW devices are, in some ways, similar to elastomers such as butyl rubber at room temperature, key differences exist. Although relatively linear with respect to strain amplitude, polymeric materials display strong frequency and temperature dependence, which must be accounted for. TMW devices, on the other hand, are affected only by the dynamic strain amplitude. Hence, it is easier to design TMW devices for applications where temperature and frequency regimes are uncertain, or inappropriate for a polymer.

From the results shown, it is clear that if the vibration levels are small (for example, in satellite jitter problems), TMW devices would not be effective. Therefore, when choosing TMW devices as a damping solution, one must consider whether the dynamic strain levels lie in the range where damping is optimised.

Further studies on the mechanical behaviour of TMW devices should focus on better understanding the relaxation effects. These studies should also attempt to explain the relaxation at low frequency dynamic loading (below 0.1 Hz). Furthermore, other loading regimes (rather than the uniaxial loading considered in this work) should be explored to determine whether the trends in the mechanical properties are similar to those observed in this article.

Acknowledgements

The authors would like to acknowledge the University of Sheffield Faculty Scholarship, which funded this research. The TMW specimens studied in this work were fabricated specifically for this work by researchers at the School of Energy and Power Engineering at Beihang University, with support from the

National Natural Science Foundation of China, Grant Numbers 51475023 and 51475021. The authors would also like to specially thank Jie Hong, Yanhong Ma, and Dayi Zhang for enabling this collaboration.

References

[1] J. Hong, B. Zhu, Y. Ma, Theoretical and experimental investigation on nonlinear characterization of metal rubber, in: ASME 2011 Turbo Expo: Turbine Technical Conference and Exposition, American Society of Mechanical Engineers, 2011, pp. 877–886.

[2] H. Ao, H. Jiang, A. Ulanov, Dry friction damping characteristics of a metallic rubber isolator under two-dimensional loading processes, Modelling and Simulation in Materials Science and Engineering 13 (4) (2005) 609.

[3] G. He, P. Liu, Q. Tan, Porous titanium materials with entangled wire structure for load-bearing biomedical applications, Journal of the mechanical behavior of biomedical materials 5 (1) (2012) 16–31.

[4] D. Childs, Space shuttle main engine high-pressure fuel turbopump rotordynamic instability problem, J Eng Power Trans ASME 100 (1) (1978) 48–57.

[5] H. Ao, H. Jiang, W. Wei, A. Ulanov, Study on the damping characteristics of mr damper in flexible supporting of turbo-pump rotor for engine, in: 2006 1st International Symposium on Systems and Control in Aerospace and Astronautics, IEEE, 2006.

[6] Zarzour, M.J., Experimental evaluation of a metal-mesh bearing damper in a high speed test rig, Master's thesis, Texas A&M University (1999).

[7] Y. Ma, Theoretical and experimental investigation on a novel adaptive squeeze film damper [in chinese], Ph.D. thesis, Beijing: School of Jet Propulsion, Beihang University (2005).

[8] B. Ertas, E. Al-Khateeb, J. Vance, Rotordynamic bearing dampers for cryogenic rocket engine turbopumps, Journal of Propulsion and Power 19 (4) (2003) 674–682.

[9] G. He, P. Liu, Q. Tan, G. Jiang, Flexural and compressive mechanical behaviors of the porous titanium materials with entangled wire structure at different sintering conditions for load-bearing biomedical applications, Journal of the mechanical behavior of biomedical materials 28 (2013) 309–319.

[10] D. Zhang, F. Scarpa, Y. Ma, J. Hong, Y. Mahadik, Dynamic mechanical behavior of nickel-based superalloy metal rubber, Materials & Design (1980-2015) 56 (2014) 69–77.

[11] Y. Ma, Q. Zhang, D. Zhang, F. Scarpa, B. Liu, J. Hong, The mechanics of shape memory alloy metal rubber, Acta Materialia 96 (2015) 89–100.

[12] A. Barnes, Improvements in machinery for woven wire mesh, Wire Industry 51 (605) (1984) 403–404.

[13] D. Zhang, F. Scarpa, Y. Ma, K. Boba, J. Hong, H. Lu, Compression mechanics of nickel-based superalloy metal rubber, Materials Science and Engineering A 580 (2013) 305–312.

[14] Y. Ma, Q. Zhang, D. Zhang, F. Scarpa, D. Gao, J. Hong, Size-dependent mechanical behavior and boundary layer effects in entangled metallic wire material systems, Journal of Materials Science 52 (7) (2017) 3741–3756.

[15] B. Zhu, Theoretical and experimental investigation on compressive mechanical and thermophysical properties of metal rubber [in chinese, Ph.D. thesis, Beijing: School of Jet Propulsion, Beihang University (2012).

[16] H. Wang, J. Rongong, G. Tomlinson, J. Hong, Nonlinear static and dynamic properties of metal rubber dampers, 2010, pp. 1301–1315.

[17] M. Zarzour, J. Vance, Experimental evaluation of a metal mesh bearing damper, Journal of Engineering for Gas Turbines and Power 122(2) (2000) 326–329.

[18] E. Al-Khateeb, J. Vance, Experimental evaluation of a metal mesh bearing damper in parallel with a structural support, Proceedings of the ASME Turbo Expo 4.

[19] J. Hou, H. Bai, D. Li, Damping capacity measurement of elastic porous wire-mesh material in wide temperature range, Journal of Materials Processing Technology 206 (1-3) (2008) 412–418.

[20] B. Zhang, Z. Lang, S. Billings, G. Tomlinson, J. Rongong, System identification methods for metal rubber devices, Mechanical Systems and Signal Processing 39 (1-2) (2013) 207–226.

[21] Y. Ma, H. Wang, H. Li, J. Hong, Study on metal rubber materials characteristics of damping and sound absorption, in: ASME Turbo Expo 2008: Power for Land, Sea, and Air, American Society of Mechanical Engineers, 2008, pp. 477–486.

[22] K. Zhang, Y. Zhou, J. Jiang, Experimental study and dynamic modeling of metal rubber isolating bearing, in: IOP Conference Series: Materials Science and Engineering, Vol. 103, IOP Publishing, 2015, p. 012048.

[23] Chandrasekhar, K., Rongong, J.A., Cross, E.J., Frequency and amplitude dependent behaviour of tangled metal wire dampers, Proceedings of International Conference on Noise and Vibration Engineering and International Conference on Uncertainty in Structural Dynamics (2014) 559–572.

[24] H. M. Jaeger, S. R. Nagel, R. P. Behringer, Granular solids, liquids, and gases, Reviews of modern physics 68 (4) (1996) 1259.

[25] Y. Ponomarev, On transformation of hysteresis in damper rings made of "metal rubber" pressure-tested wire material under precessional loading

conditions, ARPN Journal of Engineering and Applied Sciences 9 (10) (2014) 1866–1872.